Rare Metal Materials and Engineering
Volume 53, Issue 9, September 2024
Available online at www.rmme.ac.cn

Science Press

Cite this article as: Pan Chaoyang, Liu Zongde, Shen Yue, et al. Microstructure and Wear Resistance of Ni-Cr Alloy Laser Cladding Layer with High Cr Content[J]. Rare Metal Materials and Engineering, 2024, 53(09): 2438-2445. DOI: 10.12442/j.issn.1002-185X.20230814.

ARTICLE

Microstructure and Wear Resistance of Ni-Cr Alloy Laser Cladding Layer with High Cr Content

Pan Chaoyang, Liu Zongde, Shen Yue, Lu Xinjie, Mao Jie, Wang Xinyu, Li Jiaxuan

Key Laboratory of Power Station Energy Transfer Conversion and System, Ministry of Education, North China Electric Power University, Beijing 102206, China

Abstract: Four kinds of Ni-*x*Cr alloy laser cladding layers (*x*=20, 40, 60 and 80, wt%) were prepared by high-speed laser cladding technique, and the relationship between microstructure and wear resistance of Ni-Cr alloy laser cladding layers with different Cr contents was investigated. The results show that the four Ni-Cr alloy laser cladding layers all have reticulated dendritic structures. Among them, Ni-20Cr and Ni-40Cr are single-phase γ-(Ni, Cr) solid solutions, and their wear mechanisms are adhesive wear and abrasive wear. With the increase in Cr content, Ni-60Cr and Ni-80Cr are γ-(Ni, Cr) phase and Cr phase, as well as Cr-rich precipitates, and their wear mechanisms are adhesive wear, abrasive wear and fatigue wear. A moderate increase in Cr content can enhance the hardness and wear resistance of Ni-Cr alloy laser cladding layer. However, excessive addition of Cr results in the precipitation of Cr-rich precipitates. The hardness of these precipitates is 2430.4 MPa, which is lower than the hardness of the Ni-60Cr matrix (4024.86 MPa) and Ni-80Cr matrix (7022.68 MPa). A hardness transition zone exists between the Cr-rich precipitates and the matrix. Cracks are likely to initiate and expand in this zone, leading to deep spalling, which is not conducive to the wear-resistant properties of the laser cladding layer. Ni-80Cr has the highest hardness, but its high Cr content leads to a large number of penetrating cracks and Cr-rich precipitates on the surface, ultimately resulting in the worst wear resistance. Ni-60Cr exhibits the best wear resistance due to its high hardness and dense microstructure.

Key words: Ni-Cr alloy; laser cladding; Cr-rich precipitate; wear resistance

Ni-Cr alloys are widely used in industries such as aerospace and energy due to their good resistance to oxidizing acids and salts, high-temperature oxidation and sulfidation corrosion[1]. It is well known that the presence of Cr promotes the formation of a dense protective layer of Cr_2O_3 on the alloy surface, which reduces the oxidation rate of alloys[2–4]. Ni-Cr alloys are susceptible to wear and tear in corrosive environments. The addition of Cr significantly improves their mechanical properties, including strength, plastic toughness and hardness[5–6]. From an economic standpoint, Cr is more cost-effective than Ni. However, an excess of brittle primary α-Cr phases can negatively affect the mechanical properties of Ni-Cr-based alloys and lead to insufficient machinability[7]. Therefore, appropriately increasing the proportion of Cr in Ni-Cr alloys is of practical significance for improving alloy properties and reducing costs.

Usually, Ni-Cr alloys with high Cr content can only be molded by casting process[8]. Hanke[9] et al used friction cladding process to prepare a Cr60Ni40 layer on nickel-based alloy, Nimonic 80A, and demonstrated that it is feasible to prepare Ni-Cr alloy coatings with high Cr content on a ductile substrate, expanding the application range. Bozzi[10] compared the microstructure and wear resistance properties of as-cast and laser-cladded Stellite alloys. They found that laser-cladded Stellite alloys have a finer microstructure and superior wear resistance. Song[11] et al examined the corrosion properties of Ni50Cr50 alloys prepared by four methods, including cold spray, HVOLF and HVOGF thermal spray and laser cladding. The study indicates that the Ni50Cr50 coating produced by laser cladding showcases superior performance owing to its dense microstructure. Laser cladding technique is characterized by a high solidification rate, low dilution and void ratio and strong metallurgical bonding strength compared with conventional methods, which endow laser cladding layer

Received date: December 16, 2023
Corresponding author: Liu Zongde, Ph. D., Professor, Key Laboratory of Power Station Energy Transfer Conversion and System, Ministry of Education, North China Electric Power University, Beijing 102206, P. R. China, Tel: 0086-10-61772812, E-mail: lzd@ncepu.edu.cn

with fine crystal structures and new phases that are not available under equilibrium conditions. This ultimately leads to excellent properties and longevity, making it highly promising for industrial applications[12–15].

In the process of laser cladding, excessive heating and cooling rates can lead to precipitated phases in the laser cladding layer, which may have a certain influence on the performance of the laser cladding layer. Julian[16] et al did not find precipitates in the microstructure of Cr60Ni40 alloy obtained through solid solution annealing, which only consisted of two phases: Ni-rich phase and Cr-rich phase. Chen[17] et al utilized laser cladding technique to produce Cr60Ni40 laser cladding layer with the same composition, and found that there are obvious Cr-rich precipitates in the Cr60Ni40 laser cladding layer. Although the oxidation rate of Cr-rich precipitates is slow, they can cause the formation of an uneven protective chromium oxide layer on the surface, resulting in the degradation of the corrosion resistance performance.

Currently, laser cladding technique is not widely used to prepare Ni-Cr alloys with high Cr content. Researchers primarily focus on the corrosion and high-temperature oxidation resistance of Ni-Cr alloys. The relationship between the microstructure of Ni-Cr alloy laser cladding layers with high Cr content and their wear-resistant properties is not yet fully understood. In this study, Ni-*x*Cr alloy laser cladding layers with different Cr contents (*x*=20, 40, 60 and 80, wt%) were prepared on a Q235 steel substrate using laser cladding technique, the effects of Cr content on the microstructure and hardness of the Ni-Cr alloy laser cladding layers were analyzed, and the wear resistance of the laser cladding layers was evaluated by the wet-sand abrasive abrasion test, which provided theoretical references for the application of the Ni-Cr alloy laser cladding layer with high Cr content under wear conditions.

1 Experiment

1.1 Materials and laser cladding process

In this study, Q235 low carbon steel plate was selected as the substrate material and cleaned with acetone solution to eliminate rust and oil on surface. Four kinds of Ni-Cr alloy powders were prepared, named as Ni-20Cr, Ni-40Cr, Ni-60Cr and Ni-80Cr, with a particle size range of 38−75 μm, and the chemical composition of the substrate material and the cladding material is shown in Table 1. A laser cladding system (RFL-C3000S, Wuhan Riggs Fiber Laser Technology Co., Ltd) was used to prepare the Ni-Cr alloy laser cladding layer under the following parameters: power of 1800 W, operating voltage of 220 V, spot diameter of 2 mm, scanning speed of 8.33 cm/s, overlap rate of 60%, powder flow rate of 20 g/min, laser focal length of 50±0.2 mm and laser cooler temperature of 24±0.5 °C, and the powder feeding system used argon protective gas with a flow rate of 15 L/min to prevent powder oxidation during the coating process. Fig. 1 shows the schematic of high-speed laser cladding process. The Ni-Cr alloy with high Cr content is brittle and prone to cracking during the preparation process, so liquid dye penetration was used to detect the cracking morphology of the laser cladding layer. The macroscopic surface of the laser cladding layer is shown in Fig. 2, and the red penetrant penetrates the surface of Ni-80Cr, indicating that the laser cladding layer is full of cracks, while other three laser cladding layers are free of cracks. Laser cladding layers with a thickness greater than 4 mm was obtained through a multilayer cladding process, and wire cutting was used to process the laser cladding layers.

Table 1 Chemical composition of materials (wt%)

Material	Ni	Cr	Fe	Si	C
Q235	-	-	Bal.	0.34	0.16
Ni-20Cr	Bal.	20	-	-	-
Ni-40Cr	Bal.	40	-	-	-
Ni-60Cr	Bal.	60	-	-	-
Ni-80Cr	Bal.	80	-	-	-

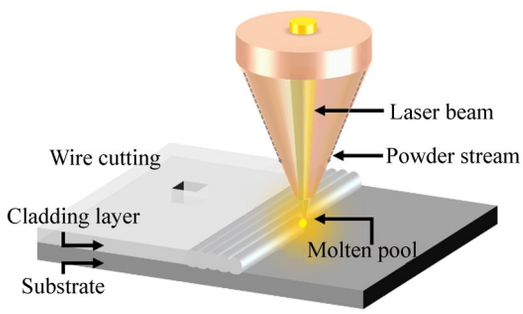

Fig.1 Schematic of the high-speed laser cladding process

1.2 Characterization method

X-ray diffractometer (XRD, Rigaku D/MAX-2400, Japan; Cu-Kα radiation, scanning range 10° – 90° , scanning rate 8°/min), scanning electron microscope (SEM, ZEISS EVO 18, Ger-many; accelerating voltage 20 kV) and energy dispersive X-ray spectroscope (EDS, Bruker Quantax, Germany) were used to analyze the phase composition, microstructure and elemental distribution of the laser cladding layer, respectively. The sample size was 10 mm×10 mm×10 mm (including substrate). Before observing the microstructure, the treated samples were subjected to surface erosion using aqua regia (HNO_3-3HCl).

1.3 Vickers hardness test

The Vickers hardness of the surface and cross-section of the laser cladding layer was measured by an FM-300 microhardness tester, with a load of 0.98 N and a loading time of 15 s at 200 μm intervals.

1.4 Wear resistance test

According to ASTM G105-20 standard, 50 mm×25 mm×4 mm sample was subjected to wear performance testing by the MLS-225 wet sand wear tester. The abrasive consisted of deionized water and SiO_2 of 212−270 μm. The rubber wheel was 178 mm in diameter and rotated at 180 r/min under a load of 70 N. The reason for choosing wet sand as abrasive is that

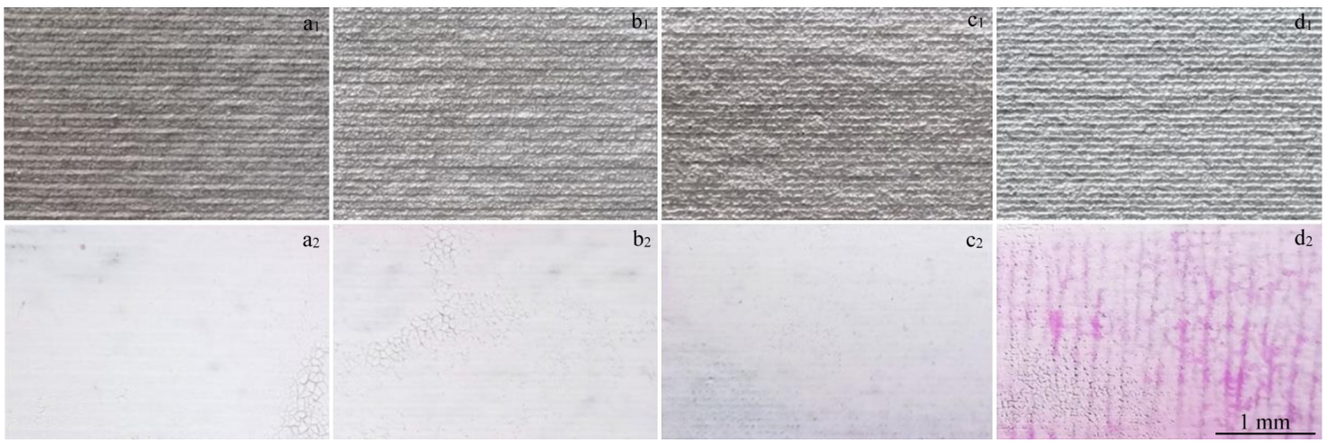

Fig.2 Macroscopic surfaces of Ni-20Cr (a_1–a_2), Ni-40Cr (b_1–b_2), Ni-60Cr (c_1–c_2) and Ni-80Cr (d_1–d_2)

water can act as a lubricant, dissipate the heat generated by friction and prevent oxidation reactions[18]. The samples were pre-ground at 2000 revolutions to eliminate experimental errors. Ten experimental cycles were set up, with each cycle consisting of 4000 revolutions. Weighing was repeated five times at the end of each cycle (accuracy 0.0001 g) and the volume loss was calculated using the following equation:

$$V = \frac{1000(W_1 - W_0)}{\rho} \quad (1)$$

where V is the volume loss (mm^3); W_1 is the mass at the end of each cycle (g); W_0 is the initial mass (g); ρ is the density (g/cm^3). Finally, the wear morphology was analyzed.

2 Results and Discussion

2.1 Microstructure and composition

Fig. 3 displays the XRD patterns of four laser cladding layers. The diffraction peaks of Ni-20Cr and Ni-40Cr correspond to the γ-(Ni,Cr) solid solution (fcc) with preferred crystal planes of (111), (200) and (220). Compared with the standard Ni peaks, the diffraction peaks of γ-(Ni, Cr) are shifted to the left at a small angle, which is due to the lattice distortion caused by the presence of Cr atoms in Ni lattices in the form of solutes, resulting in larger lattice constants and thus causing the shift of the diffraction peaks. The phenomenon of diffraction peak shift can be explained by Bragg's equation: $2d\sin\theta=\lambda$, where d represents the distance between crystalline planes, θ represents the angle between incident light and crystalline planes, and λ is the wavelength of the Cu target.

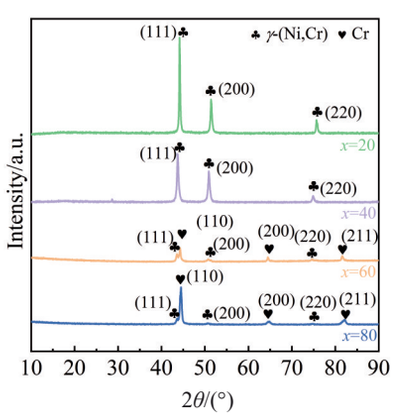

Fig.3 XRD patterns of different Ni-xCr alloys

With the increase in Cr content, the matrix element of Ni-Cr alloy starts to change from Ni to Cr. In addition to the presence of γ-(Ni, Cr) peaks, Cr peaks can be detected in Ni-60Cr and Ni-80Cr alloys, whose preferred crystal planes are (110), (200) and (211). The shift of the γ-(Ni, Cr) peak is more significant due to the higher saturation of Cr atoms in the γ-(Ni, Cr) solid solution, leading to a higher degree of lattice distortion in γ-(Ni, Cr). During the cooling process, the solubility of Ni atoms in the Cr matrix decreases, resulting in no significant shift of the Cr peaks. Additionally, the relative intensity of the Cr peaks of Ni-80Cr is higher than that of Ni-60Cr.

Fig. 4 shows the reticulated dendritic structures that are typical in laser cladding layers. The primary phase, which appears dark gray, is surrounded by the eutectic phase, which appears light gray. In Ni-20Cr and Ni-40Cr alloys, the dark gray primary phase is Ni-rich, while the light gray eutectic phase is Cr-rich. The Cr-rich phases account for 26.86% and 38.35% of the matrix in Ni-20Cr and Ni-40Cr alloys, respectively. The EDS results of different areas are listed in Table 2. The Cr content in the primary phases (area 1 and 4) is lower than that in the eutectic phases (area 2 and 3). Dendritic segregation causes compositional differences, resulting in different colors after etching. The solidification speed of laser cladding is fast, and some Cr atoms do not have enough time to diffuse and to solidify into the γ-Ni lattice[19]. As a result, they are enriched in the intergranular region. Additionally, a few micropores are visible in the laser cladding layer due to the delayed escape of the protective gas.

As the Cr content increases, the microstructure of Ni-Cr alloys with Cr as the matrix element changes. Black precipitates appear on the surface, with the size ranging from 15 μm to 30 μm. These precipitates are mainly composed of Cr atoms, and a few Ni atoms. The melting point of Cr is higher than that of Ni. During the laser cladding process, Cr undergoes solidification firstly, and the solubility of Ni in Cr is also relatively low. As a result, excess Cr cannot form a

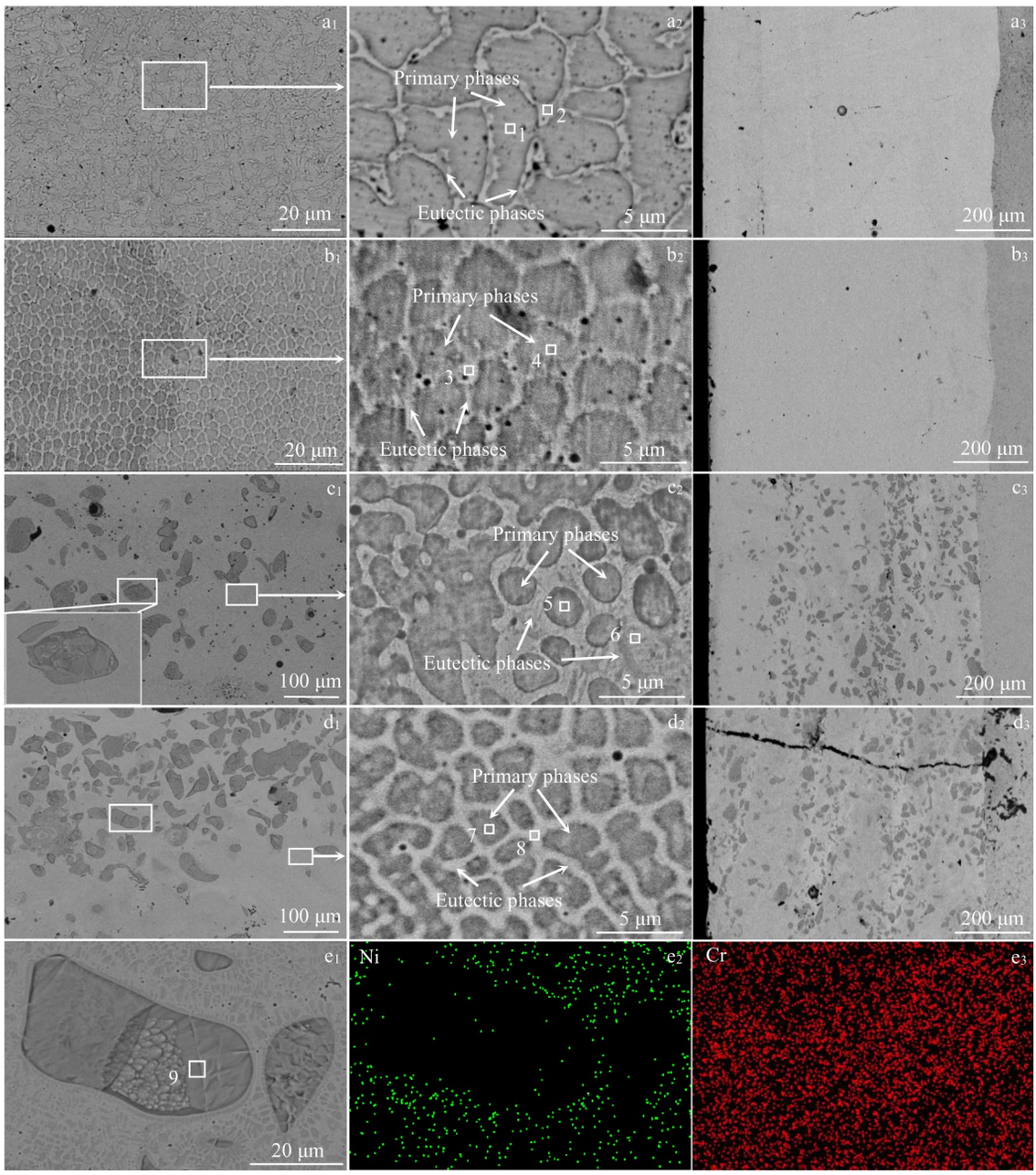

Fig.4 Surface morphologies (a_1–d_1 and a_2–d_2) and cross-sectional (a_3–d_3) morphologies of Ni-20Cr (a_1–a_3), Ni-40Cr (b_1–b_3), Ni-60Cr (c_1–c_3) and Ni-80Cr (d_1–d_3); Cr-rich precipitate (e_1) and corresponding EDS mappings of element Ni (e_2) and Cr (e_3)

Table 2 EDS results of different areas in Fig.4 (wt%)

Area	1	2	3	4	5	6	7	8	9
Ni	79.43	67.92	53.64	58.60	34.74	47.64	17.58	36.40	0
Cr	20.57	32.08	46.36	41.40	65.26	52.36	82.42	63.60	100

solid solution with Ni completely, leading to the formation of Cr-rich precipitates directly in the Ni-Cr alloy[17]. The area fractions of each phase in Ni-60Cr and Ni-80Cr are analyzed: the Cr-rich precipitates in Ni-60Cr account for 15.03% and the matrix accounts for 84.97%; the fraction of Cr-rich precipitates in Ni-80Cr is 23.36% and that of the matrix is 76.64%. The results indicate that the higher the Cr content, the higher the amount of Cr-rich precipitate in the Ni-Cr alloy laser cladding layer. The matrix of both Ni-60Cr and Ni-80Cr exhibits a reticulated dendritic structure. Combined with the EDS results, it is evident that the primary phase in dark gray is rich in Cr, while the eutectic phase in light gray is rich in Ni. The Cr-rich phases in Ni-60Cr and Ni-80Cr account for 56.30% and 65.26% of the matrix, respectively.

Fig. $4a_3 - 4d_3$ display the cross-sectional morphologies of four laser cladding layers. Ni-20Cr, Ni-40Cr and Ni-60Cr exhibit a dense microstructure with a few air holes. In contrast, the Ni-80Cr laser cladding layer has defects such as holes and cracks at the boundary of the substrate, as well as noticeable penetrating cracks on the surface. This is because

the Cr-rich phase in the Ni-Cr alloy matrix usually exhibits high hardness and brittleness. Excessive Cr can also increase the proportion of Cr-rich phase in the Ni-Cr alloy matrix, leading to poor mechanical properties of the Ni-Cr alloy and easy initiation and propagation of cracks[7,20].

2.2 Vickers hardness

Fig. 5 displays the microhardness variation of each sample with respect to the distance from the laser cladding layer surface. The overall microhardness of Ni-80Cr is the highest, ranging within 6958–7350 MPa, and that of Ni-60Cr is 3734–4307 MPa. The microhardness of Ni-40Cr is approximately 2156 MPa, while that of Ni-20Cr is the lowest about 1960 MPa. The difference in microhardness between Ni-20Cr and Ni-40Cr is small, resulting in a relatively smooth overall microhardness change. Through microstructure and microstructure analysis, Ni-20Cr and Ni-40Cr are dominated by γ-(Ni, Cr) solid solution with low microhardness. In addition, the atomic radii of Cr and Ni are close to each other, the degree of lattice distortion in the formation of γ-Ni solid solution is small, and the solid solution strengthening effect is limited, so the hardness of Ni-40Cr is not obviously enhanced compared to that of Ni-20Cr.

As the Cr content continues to increase, the hardness begins to rise sharply. Compared with Ni-40Cr and Ni-20Cr, Ni-60Cr and Ni-80Cr with high Cr content possess more Cr-rich phases. The Cr-rich phase usually exhibits high hardness, which plays a crucial role in improving the hardness of Ni-Cr alloys. Ni-80Cr has more Cr-rich phases (65.26%), so it exhibits the highest microhardness.

The surface microhardness was analyzed separately, and the measurement results are shown in Fig.6. It is worth noting that the microhardness error values of Ni-60Cr and Ni-80Cr are relatively large compared with that of Ni-20Cr and Ni-40Cr. The microhardness fluctuation phenomenon may be related to the Cr-rich precipitates in Ni-60Cr and Ni-80Cr. The surface microhardness of four laser cladding layers is consistent with the cross-section microhardness. However, the microhardness of Cr-rich precipitates is only 2430.4 MPa, which is very lower than the matrix hardness of Ni-60Cr (4024.86 MPa) and

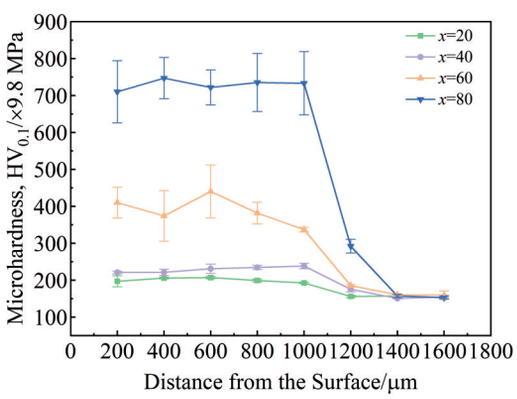

Fig.5 Cross-section microhardness of Ni-*x*Cr alloy laser cladding layers

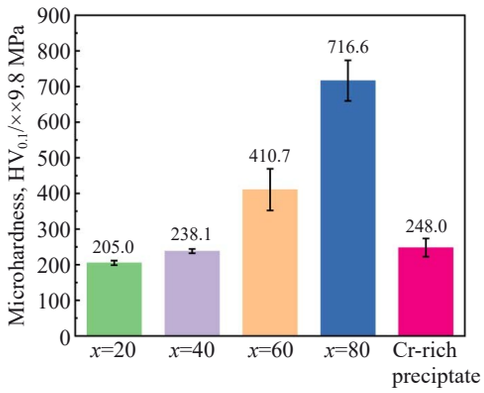

Fig. 6 Surface microhardness of Ni-*x*Cr alloy laser cladding layers and Cr-rich precipitate

Ni-80Cr (7022.68 MPa). The microhardness of Ni-20Cr and Ni-40Cr is lower, which is 2009 and 2333.38 MPa, respectively. Fig.7 presents the Vickers hardness indentation morphology of Cr-rich precipitates and different matrixes, confirming the microhardness measurements. According to Conrath[21], the addition of Cr does not completely and monotonically increase the hardness of Ni-Cr alloys. Instead, it results from the superposition of the hardness of the Cr-rich phase and the hardness of the Ni-rich phase. As the Cr content increases, the microhardness of Ni-Cr alloy will also increase. Therefore, the microhardness of Cr-rich precipitates with 100wt% Cr content is lower than that of Ni-60Cr matrix and Ni-80Cr matrix. However, when the Cr content reaches a critical value, the microhardness of Ni-Cr alloy will continue to decrease. For different preparation processes, this critical value may vary.

2.3 Wear resistance

Fig. 8 shows the wear curves of four laser cladding layers. The wear process is not entirely a standard linear law, so a

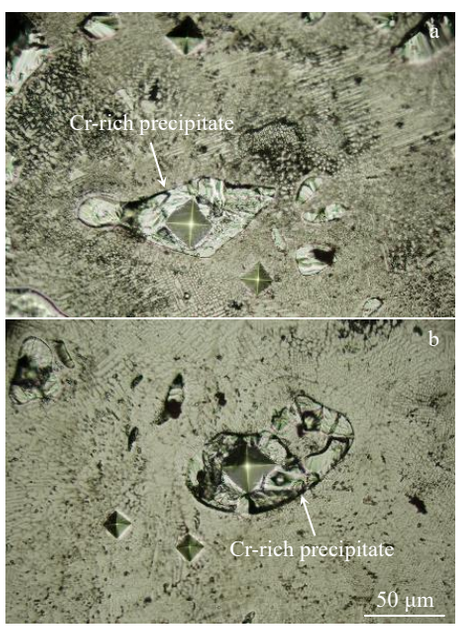

Fig.7 Vickers hardness indentation morphologies of Ni-60Cr (a) and Ni-80Cr (b)

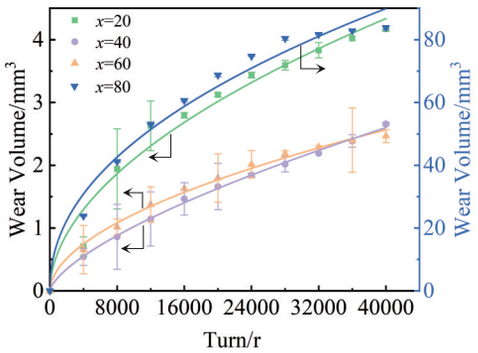

Fig.8 Wear volume loss curves of Ni-*x*Cr alloy laser cladding layer

non-linear fitting is performed on the wear curve using the following formula:

$$V = aT^n \quad (2)$$

where a and n are constants; V represents the volume loss; T represents the number of turns. The results show that the volume loss increases gradually as the number of turns increases. According to the difference in wear rate, the wear curves can be divided into two stages, i. e., the running-in stage and the stable wear stage. In the running-in stage, the sample is just in contact with the abrasive grains and the wear rate is usually faster. As the abrasive grains continuously come into contact, the friction surface is gradually smoothed and the actual contact area is enlarged, leading to a decrease in the wear rate. At the same time, as the wear process continues, strain hardening effects occur on the surface, and the stable wear stage is reached[22]. The volume loss in the stable wear stage increases almost linearly. The wear volume and the fitting results of wear curve are shown in Table 3. R^2 values indicate the quality of the fitting results. According to the volume loss, the wear resistance is evaluated as follows: Ni-60Cr> Ni-40Cr >Ni-20Cr >Ni-80Cr.

Fig. $9a_1-9a_2$ display the surface morphologies of Ni-20Cr after wear. The wear volume loss of Ni-20Cr is 4.1788 mm^3. Long and deep grooves are visible on the surface of Ni-20Cr, and the edges of the grooves produce a material buildup. This indicates that the abrasive grains have caused a severe ploughing effect on the surface of the material, which is a characteristic of abrasive wear[23]. Microcracks and adhesive layer are visible on the surface, which indicates that adhesive wear also occurs on the sample. The EDS results of different areas are listed in Table 4. Area 1 of the adhesive layer exhibits a high concentration of O and Si, indicating the possibility of wear debris adhering to the wear surface[24]. The wear resistance of Ni-40Cr is marginally superior to that of Ni-20Cr, with the wear volume loss of 2.6575 mm^3. Fig. $9b_1-9b_2$ illustrate that the grooves on the surface of Ni-40Cr become shallower, and the microcracks and adhesive layer are significantly weakened. Small abrasive debris can also be observed during the wear process, which can cause more serious damage to the sample. However, the effect of the abrasive debris is essentially negligible compared with the effect of the initial abrasive grains size.

Table 3 Wear volume and the fitting results of wear curve

Sample	Wear volume/mm^3	Fitting of wear curve	R^2
Ni-20Cr	4.1788	V=0.0168$T^{0.5238}$	0.968
Ni-40Cr	2.6575	V=0.0021$T^{0.6725}$	0.998
Ni-60Cr	2.4650	V=0.0087$T^{0.5362}$	0.993
Ni-80Cr	83.8460	V=0.6574$T^{0.4641}$	0.978

When the Cr content is low (Ni-20Cr and Ni-40Cr), the Ni-Cr alloy laser cladding layer is dominated by the γ-(Ni, Cr) solid solution. This solid solution has good plasticity and low hardness. When subjected to the normal force exerted by the abrasive grain, the sample surface is prone to plastic deformation. If the deformation exceeds its tensile limit, the surface will form cracks and collapse downward. Under repeated contact stress, the cracks will expand and cause shallow spalling. Meanwhile, the abrasive particles generate relative motion tangentially to the friction surface, resulting in the formation of grooves and adhesive layer[22]. The wear mechanisms of Ni-20Cr and Ni-40Cr are abrasive and adhesive wear.

Ni-60Cr exhibits the best wear resistance, with the wear volume loss of 2.4650 mm^3. Shallow and short grooves, as well as adhesion layers, are visible on the surface in Fig. $9c_1-9c_2$. In contrast to Ni-20Cr and Ni-40Cr, deeper spalling pits with dimensions similar to Cr-rich precipitates are present on the surface of Ni-60Cr, indicating that spalling of Cr-rich precipitates may have occurred. Additionally, expanding microcracks are observed around the spalling pits. EDS analysis of the pits reveals that area 6 has a high Cr content of 97.73wt%, suggesting the presence of Cr-rich precipitates in this area. Areas 7–9 have Cr contents of 63.72%, 57.54% and 56.62%, respectively, suggesting that spalling of the craters occurs not only in the Cr-rich precipitates but also in the matrix. The Ni-80Cr sample exhibits the worst abrasion resistance, with the wear volume loss of 83.8460 mm^3. As shown in Fig. $9d_1-9d_2$, the surface of the Ni-80Cr sample is characterized by shallow, short grooves, adhesion layers and more pronounced deep pits. A transverse penetration crack is observed, which exists prior to the wear test. The area where the craters are located has a Cr content of 100wt%, without other elements present, indicating exfoliation of intact Cr-rich precipitate. As the Cr content increases (Ni-60Cr and Ni-80Cr), the Ni-Cr alloy laser cladding layer is dominated by Cr-rich phases, resulting in a significant increase in hardness and improved resistance to surface plastic deformation[25]. Consequently, the extrusion and cutting effect of abrasive grains on the sample surface are weakened, leading to shorter and shallower grooves and a thinner adhesive layer. It should be noted that the Ni-60Cr and Ni-80Cr surfaces show deeper spalling pits, which are actually the spalling of Cr-rich precipitates.

The Cr-rich precipitates have a lower hardness (2430.4 MPa) than the matrix, which leads to a hardness transition zone between them. This transition zone is prone to generation and expanding of initial cracks under long-term contact stress, ultimately leading to fatigue damage and the formation of deeper spalling pits[26]. The wear mechanisms of Ni-60Cr and

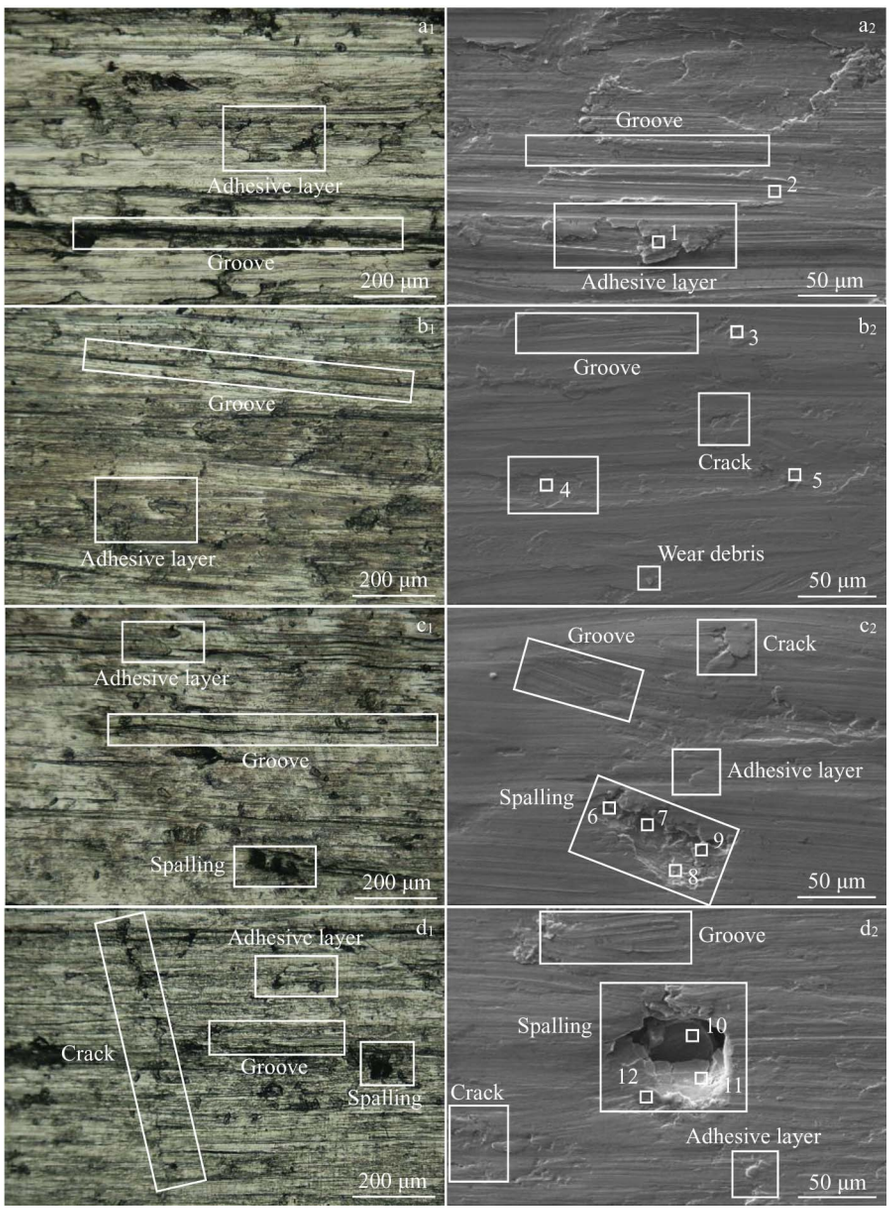

Fig.9 Surface morphologies of Ni-20Cr (a_1–a_2), Ni-40Cr (b_1–b_2), Ni-60Cr (c_1–c_2), and Ni-80Cr (d_1–d_2) after wear test

Table 4 EDS results of different areas in Fig.9 (wt%)

Area	1	2	3	4	5	6	7	8	9	10	11	12
Ni	35.58	77.11	56.30	54.82	23.41	1.72	34.40	38.73	37.63	0	25.18	16.86
Cr	11.04	20.12	39.36	36.07	16.83	97.73	63.72	57.54	56.62	100	73.35	68.76
O	31.35	0.36	3.31	5.10	29.02	0.11	1.02	2.63	4.13	0	0	8.07
Si	22.03	2.41	1.03	4.01	30.74	0.44	0.86	1.10	1.62	0	1.47	6.31

Ni-80Cr include abrasive wear, adhesive wear and fatigue wear. The area fraction of Cr-rich precipitates in Ni-80Cr differs by 8.33% from that of Ni-60Cr. Although Ni-80Cr has the highest hardness, it exhibits the worst wear resistance, which may be attributed to the presence of numerous macro-cracks. The expansion rate of abrasive grains is much faster when they come into contact with these macro-cracks compared with in contact with micro-cracks, resulting in more significant volume loss.

3 Conclusions

1) The surface microstructures of the four kinds of Ni-Cr alloy laser cladding layers are all composed of primary and eutectic phases with a reticulated dendritic structure, and there is elemental segregation between the two phases. Ni-20Cr and Ni-40Cr are single-phase γ-(Ni, Cr) solid solutions, and Ni-60Cr and Ni-80Cr consist of γ-(Ni,Cr) phases and Cr phases. Cr-rich precipitates appear in the Ni-60Cr and Ni-80Cr and

the amount increases with the increase in Cr content. Except for Ni-80Cr, the microstructure of other three laser cladding layers is uniform and dense, while Ni-80Cr has a large number of defects such as penetrating cracks and holes.

2) The microhardness of Ni-20Cr and Ni-40Cr is lower, 2009 and 2333.38 MPa, respectively. As the Cr content increases, more Cr-rich phases appear in the laser cladding layer, resulting in a significant increase in the microhardness of Ni-60Cr (4024.86 MPa) and Ni-80Cr (7022.68 MPa). However, this also causes the precipitation of low-microhardness Cr-rich precipitates (2430.4 MPa).

3) The wear resistance is evaluated by wear volume loss as follows: Ni-60Cr>Ni-40Cr>Ni-20Cr>Ni-80Cr. The wear mechanisms of Ni-20Cr and Ni-40Cr are abrasive and adhesive wear, and the wear mechanisms of Ni-60Cr and Ni-80Cr include abrasive wear, adhesive wear and fatigue wear. There is a hardness transition zone between the Cr-rich precipitates and the cladding matrix. This zone is prone to initiation and expansion of cracks, which can result in deep spalling and reduce wear resistance. Ni-60Cr exhibits the best wear resistance due to its high hardness and dense microstructure.

References

1 Sequeira C A C, Cardoso D S P, Amaral L *et al. Corrosion Reviews*[J], 2016, 34: 187
2 Wang Xinyu, Liu Zongde, Cheng Kehan *et al. Corrosion Science*[J], 2023, 216: 111102
3 Sun Hua, Zhang Peng, Wang Jianqiang *et al*. *Corrosion Science*[J], 2018, 143:187
4 Gao Yuan, Liu Zongde, Wang Qi *et al. Rare Metal Materials and Engineering*[J], 2019, 48(12): 3846
5 Keskar N, Mani Krishna K V, Gupta C *et al. Materials Today Communications*[J], 2022, 33: 104831
6 Li Jiahong, Kong Dejun. *Materials*[J], 2018, 11: 137
7 Zheng Liang, Xiao Chengbo, Zhang Guoqing *et al. Journal of Alloys and Compounds*[J], 2012, 527: 176
8 Herda W, Swales G L, Tschentke *et al. Materials and Corrosion*[J], 1968, 19: 679
9 Hanke S, Beyer M, Silvonen A *et al. Wear*[J], 2013, 301: 415
10 Bozzi A C, Ramos F D, Vargas D B O. *Wear*[J], 2023, 534–525: 204857
11 Song B, Voisey K T, Hussain T. *Surface and Coatings Technology*[J], 2018, 337: 357
12 Siddiqui A A, Dubey A K. *Optics & Laser Technology*[J], 2021, 134: 106619
13 Liang Y, Liao Z Y, Zhang L L *et al. Optics & Laser Technology*[J], 2023, 164: 109472
14 Arif Z U, Khalid M Y, Rehman E U *et al. Journal of Manufacturing Processes*[J], 2021, 68B: 225
15 Zhu Lida, Xue Pengsheng, Lan Qing *et al. Journal of Manufacturing Processes*[J], 2021, 138: 106915
16 Julian Krell, Arne Röttger, Werner Theisen. *Wear*[J], 2019, 432–433: 102924
17 Chen Shanshan, Liu Zongde, Ning Huaqing *et al. Materials Letters*[J], 2023, 342: 134352
18 Bingley M S, Schnee S. *Wear*[J], 2005, 258: 50
19 Wang Qinying, Bai Shulin, Zhao Yunhong *et al. Applied Surface Science*[J], 2014, 303: 312
20 Shi Bowen, Li Tao, Guo Zhiwei *et al*. *Optics & Laser Technology*[J], 2022, 149: 107805
21 Conrath E, Berthod P. *Materials at High Temperatures*[J], 2016, 33: 189
22 Li Jiaxuan, Liu Zongde, Ning Huaqing *et al*. *Surface and Coatings Technology*[J], 2023, 474: 130068
23 Xia Yelin, Huang Zhaozhen, Chen Hanning *et al. Rare Metal Materials and Engineering*[J], 2021, 50(11): 2901 (in Chinese)
24 Zhou Kai, Xie Faqin, Wu Xiangqing *et al. Rare Metal Materials and Engineering*[J], 2021, 50(8): 2831 (in Chinese)
25 Li Gang, Zhang Jingbo, Wen Ying *et al. Rare Metal Materials and Engineering*[J], 2018, 47(6):1830 (in Chinese)
26 Roy T, Lai Q, Abrahams R *et al*. *Wear*[J], 2018, 412–413: 69

高Cr含量的Ni-Cr合金激光熔覆层组织与耐磨性能

潘朝阳，刘宗德，申　越，路鑫杰，毛　洁，王鑫宇，李家璇

(华北电力大学 电站能量传递转化与系统教育部重点实验室，北京 102206)

摘　要：采用高速激光熔覆技术制备了4种Ni-*x*Cr合金熔覆层（*x*=20、40、60和80，质量分数），研究了不同Cr含量的Ni-Cr合金熔覆层的显微组织与耐磨性能的关系。结果表明，4种Ni-Cr合金熔覆层的组织均为网状枝晶结构。其中，Ni-20Cr和Ni-40Cr为单相的*γ*-(Ni, Cr)固溶体，其磨损机制为粘着磨损和磨粒磨损。随着Cr含量的增加，Ni-60Cr和Ni-80Cr为*γ*-(Ni, Cr)相和Cr相，且存在富Cr沉淀物，磨损机制为粘着磨损、磨粒磨损和疲劳磨损。适度增加Cr含量可以提高Ni-Cr合金熔覆层的硬度和耐磨性。然而，过量添加Cr会导致富Cr沉淀物的析出。这些沉淀物的硬度为2430.4 MPa，低于Ni-60Cr基体（4024.86 MPa）和Ni-80Cr基体（7022.68 MPa）的硬度。富Cr沉淀物与熔覆层基体之间存在硬度过渡区，裂纹极易在过渡区萌生并扩展，造成深层剥落，不利于熔覆层的耐磨性能。Ni-80Cr的硬度最高，但其Cr含量过高导致表面存在大量的贯穿性裂纹和较多的富Cr沉淀物，最终表现出最差的耐磨性能。Ni-60Cr拥有较高硬度和致密的微观结构，因此表现出最好的耐磨性能。

关键词：Ni-Cr合金；激光熔覆；富Cr沉淀物；耐磨性能

作者简介：潘朝阳，男，1999年生，硕士，华北电力大学电站能量传递转化与系统教育部重点实验室，北京 102206，电话：010-61772277，E-mail：yang_1249359201@163.com